ACS APPLIED NANO MATERIALS

www.acsanm.org

Article

Development and Characterization of Nanoscale Gel-Core Liposomes Using a Short Self-Assembled Peptide Hydrogel: Implications for Drug Delivery

Geneviève Duché,* Celine Heu, and Pall Thordarson

Cite This: *ACS Appl. Nano Mater.* 2023, 6, 14745−14755

Read Online

ACCESS | Metrics & More | Article Recommendations | Supporting Information

ABSTRACT: Targeted drug delivery systems, delivering drugs to specific locations, are an emerging research interest spanning the fields of nanotechnology, bionanotechnology, and precision medicine. Topical or transdermal delivery has many advantages over traditional injection and oral delivery. Not only can it reduce the risk of systemic exposure and overdose but also it is better tolerated by certain patients. However, skin penetration remains a challenge given the protection conferred by the outermost skin layer (*stratum corneum*), preventing foreign materials, such as pathogenic substances, from infiltrating the body. A promising alternative to overcome the *stratum corneum* delivery challenge combines the self-assembling properties of nanoscale systems, like liposomes, with peptide hydrogelators, creating an effective topical drug delivery system that couldcross the protective skin barrier. Presented herein is the successful production of gel-core liposomes using two short self-assembled peptide hydrogels. The subsequent composite gel-core liposomes were extensively characterized using a range of techniques including microscopy and SANS.

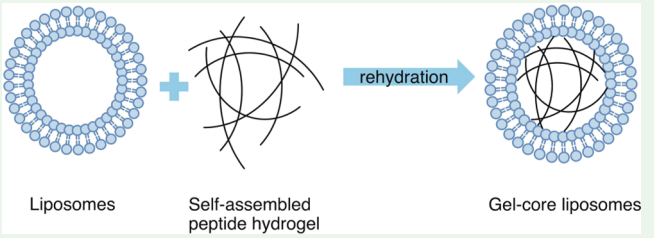

KEYWORDS: *hydrogel, liposomes, self-assembly, AFM, gel-core liposomes, delivery, characterization*

1. INTRODUCTION

Nanoscale systems combining both gels and liposomes, such as gels inside liposomes (termed gel-core liposomes), are of growing interest. These new materials provide novel approaches to new materials with unusual properties by combining advantages conferred by both the gel and liposome structure. Materials developed optimizing these properties will enable topical drug delivery systems, capable of bypassing the *stratum corneum* (outermost layer of skin, made of horny, keratinized dead cells).[1]

Gels, though having a long history, remain a material difficult to precisely define and without a technically rigorous generally accepted formal definition. They are usually described as a two-component system consisting of a three-dimensional (3D) matrix of fibers encapsulating a solvent, with the solvent often composing the majority of the gel.[2] Self-assembled hydrogels, also referred to as supramolecular hydrogels, consist of low molecular mass organic gelators, such as peptides, in water.[3] Hydrogels, with their important industrial relevance, particularly in the cosmetics industry as topical products, are the focus of this study. They are also gaining relevance in the pharmaceutical industry for their ease of application, accessibility, biocompatibility, and drug delivery capabilities.[4] Furthermore, hydrogels have greater appeal to patients compared to topical systems such as creams or ointments, as they leave no sticky residue on the skin, are easily removed with water, and administration can be stopped at any time.[5] Despite the advantages of hydrogels as topical drug delivery systems, few reports exist on their use in topical drug delivery. Previous reports on hydrogels used for topical release noted significant impediments to *stratum corneum* penetration without prior treatment,[6] reinforcing the necessity of a two-component system.

Liposomes, or lipid vesicles, are spherical polymolecular aggregates generally formed in an aqueous solution in the presence of a dry lipid film.[7] As their complex structure incorporates both hydrophilic and hydrophobic compartments, additives can be compartmentalized and transported. Hydrophilic components localize within the inner aqueous phase, while lipophilic components accumulate within the bilayer walls. Thus, the sections separate potentially reactive components and minimize the encapsulated material decomposition.[8] These systems also present good biodegradability, biocompatibility, and low toxicity, which are ideal drug delivery system characteristics.[9] Phospholipid liposomes are also reported to readily interface with skin lipids, presenting an

Received: May 16, 2023
Accepted: July 28, 2023
Published: August 10, 2023

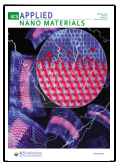

https://doi.org/10.1021/acsanm.3c02172
ACS Appl. Nano Mater. 2023, 6, 14745−14755

Scheme 1. Visual Representation of Gel-Core Liposomes and Its Components

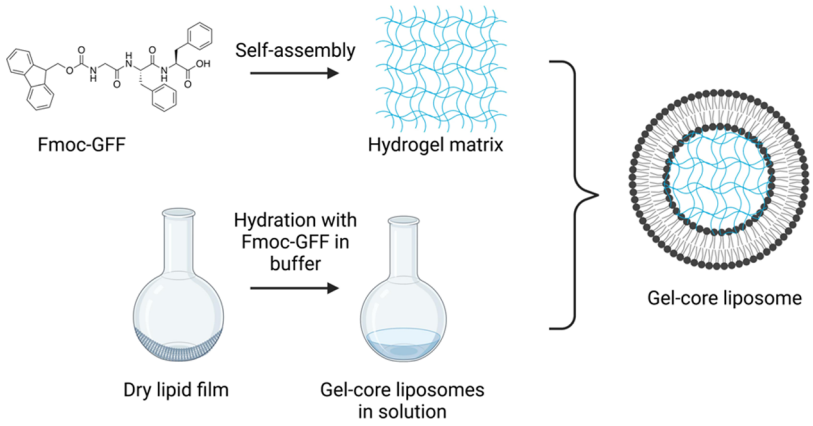

interesting and versatile transdermal delivery vector.[10] However, these liposomes are vulnerable to physical disruption, with vesicle aggregation, fusion, and rupture resulting in uncontrolled and rapid drug release, decreasing drug efficacy and yielding potential off-target effects.[11] Thus, addressing liposome structural weakness is essential to develop robust liposome drug delivery systems with controlled or delayed-release profiles.

One strategy to overcome liposome structural weaknesses is to use the rigidity of gels to reinforce structural definition. By combining gels and liposomes within a composite system, drug delivery may be improved and enable precisely controlled drug release.[6] Aqueous gel-core inclusion within liposomes (forming gel-core liposomes) is known to improve mechanical properties, stability, and influence release patterns.[12] Several examples exist of gel-core liposome systems using either polymeric gels[9,12] or biopolymeric gels.[6,10] Previous reports of hybrid lipid−peptide systems yielding micelles and cubosomes proved to be viable targeted drug delivery systems.[13,14] However, no examples of gel-core liposome systems incorporating self-assembled peptide hydrogels are reported.

Self-assembled peptide hydrogels confer many advantages over polymeric or biopolymeric gels, including being chemically well-defined, high encapsulation efficiency, improved biocompatibility for the absence of cross-linkers, and nontoxic degradability.[15] Self-assembled peptide hydrogels are unique in their sole reliance upon noncovalent intermolecular forces such as $\pi-\pi$ stacking or hydrogen bonding to form their gel state.[16] This avoids the use of cross-linkers that may compromise the gel biocompatibility. Furthermore, the peptide hydrogel structure presents advantages, over both synthetic and naturally derived hydrogels, as they are composed only of naturally occurring amino acids.[17]

In this work, the peptide gelator Fmoc glycine diphenylalanine (Fmoc-GFF), was selected for its relatively good biocompatibility, ease of synthesis, and similarity to other well-known short peptide gelators such as Fmoc-diphenylalanine (Fmoc-FF).[18,19] Though less studied than other peptide sequences, Fmoc-GFF is advantaged by the reduced hydrophobicity of the glycine residue, which increases gelation pH. This increases gel biocompatibility, supporting its use in this study.[20] The Fmoc group, as an N-terminal capping group, is extensively studied and enhances gelation efficiency by promoting $\pi-\pi$ stacking.[21] Herein, we report the formation and characterization of gel-core liposomes using the Fmoc-GFF self-assembled small peptide hydrogelator.[22]

2. EXPERIMENTAL SECTION

All reagents were purchased from Chem-Impex International, Nova Biochem, Auspep, Sigma-Aldrich, Avanti Polar Lipids, Inc., and Sapphire Bioscience and used without modification unless specified. Phosphate buffer solution (PBS) was prepared using stock solutions of sodium dihydrogen phosphate (0.1 M) and disodium hydrogen phosphate (0.1 M) diluted with Milli-Q water or by dissolving PBS tablets in the corresponding volume of Milli-Q water to reach a final concentration of 20 mM. The pH was then adjusted with aqueous solutions of sodium hydroxide and hydrochloric acid.

The Fmoc-GFF peptide gelators were synthesized following standard solid-phase peptide synthesis protocols previously developed using a 2-chlorotrityl chloride resin, with HBTU and HOBt as coupling reagents.[20] Amide coupling completion was determined using a ninhydrin-based Kaiser test. Mixtures were then purified by semipreparative HPLC using a Shimadzu Prominence UFLC HPLC system and then lyophilized yielding the hydrogelators as a powder. The resulting Fmoc-GFF solutions were made of 0.5% (w/v) Fmoc-GFF in PBS buffer (20 mM, pH 7.4). The Fmoc-GFF solutions were vortexed, sonicated, and heated to ca. 40−60 °C before allowing to cool in ambient conditions and undergo gelation. Gelation was confirmed by an inversion test.

Liposomes were prepared following a thin film hydration method. Egg phosphatidylcholine (egg-PC) and cholesterol (1:0.15) were dissolved in chloroform. The solvent was removed under reduced pressure in a rotary evaporator until complete removal to obtain a thin film on the flask wall. The dry film was then hydrated with PBS (20 mM, pH 7.4) to reach a final lipid concentration of 15 mg/mL. Rehydration was ensured by using vortex mixing and sonication. The solution was then extruded at room temperature through polycarbonate membranes with a pore size of 400 nm and then 200 nm at room temperature. Gel-core liposomes (see Scheme1) were prepared using the same method except for the rehydrating buffer. The dry lipid film was rehydrated using a solution of Fmoc-GFF (1% (w/v)) made by dissolving the gelator in PBS buffer (pH 10.0) to reach a final lipid concentration of 15 mg/mL. Once extruded, the solution was dialyzed overnight against PBS pH 5.4 to ensure gelation inside the liposomes and solution pH reduction to 7.4. Dispersions were then hermetically sealed and stored at 4 °C.

Biotinylated liposomes and gel-core liposomes were prepared by following the same methods. Biotinylated egg-PC (1 mol % of the total egg-PC volume) was added during the formation of the thin lipid film.

2.1. Characterization. The average diameter size and polydispersity index (PDI) of liposomes and gel-core liposomes were measured via dynamic light scattering (DLS) using a Malvern Zetasizer Nano ZS. Liposomes and gel-core liposome samples for DLS were dissolved 100-fold in PBS buffer (20 mM, pH 7.4). The solution was left to equilibrate at room temperature for 5 min. Measurements were taken using a viscosity of 0.8872 cP and refractive indices of 1.330 and 1.45 for lipids.

https://doi.org/10.1021/acsanm.3c02172
ACS Appl. Nano Mater. 2023, 6, 14745−14755

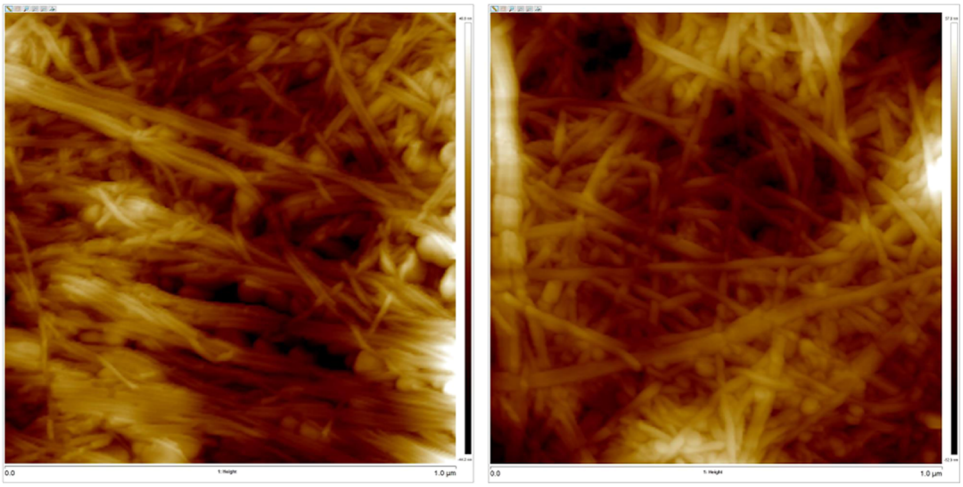

Figure 1. AFM images of dried-out sample of Fmoc-GFF gels on a mica substrate formed in 20 mM PBS buffer at pH 7.4 and 1/12 of the normal concentration. Images were obtained on a Bruker MultiMode 8.

Transmission electron microscopy (TEM) micrographs were recorded on a JEOL 1400 (100 kV) and an FEI Tecnai GG2 20 (200 kV). A drop of sample was cast onto a carbon-coated grid and left for 1 min before blotting. The grid was then negatively stained using 2% uranyl acetate for 1 min and then blotted. *Cryo*-TEM micrographs were recorded on an FEI Tecnai G2 20 (200 kV) with samples prepared by an EM GP vitrification robot by Leica Microsystems. A drop of sample was cast onto a glow-discharged holey support carbon-coated grid, left to sit for 30 s, blotted for 1.8 s, left to sit for 1.0 s, and then plunged into liquid ethane. The grids were maintained under liquid nitrogen to avoid thawing and ice formation, which could impact imaging.

Confocal microscopy was performed on a Leica SP5 2 P STED instrument with a fluorescent optically active hydrogelator. For confocal imaging, liposomes with cores of the optically active perylene gelator (*N*′-alanyl-perylene-3,4,9,10-tetracarboxylic monoimide dibutyl ester)[1] were used. These were formed following a previously described protocol. Within 2 days of liposome formation, the suspension was highly diluted (1%) before being dispersed in Fmoc-GFF (1% (w/v)) and imaged on a concave glass slide with a coverslip.

Atomic force microscopy (AFM) was performed on a Bruker Multimode 8 and Bruker Bioscope Catalyst. For dry liposome imaging, a small sample droplet was air-dried on a mica sheet overnight before imaging at room temperature using PeakForce Tapping. For solution imaging, liposomes were modified using biotinylated egg-PC (1 mol % of the total egg-PC volume). AFM surfaces were prepared for immobilization as follows: mica disks were freshly cleaved, and glass slides were cleaned for 2 h in aqueous potassium hydroxide (2 M). Glass slides were then rinsed using ethanol and Milli-Q water. Surfaces were then covered with a solution of streptavidin (17 mg/mL) in PBS buffer (20 mM, pH 7.4) to which acetic acid (20%) was added, for at least 1 h, and no longer than 2 h. Surfaces were then dried under a gentle stream of nitrogen. The liposomal solution (40 μL) was then cast on the surfaces and allowed to settle for 40 min. Excess liquid (20 μL) was removed and replaced with fresh PBS buffer (20 μL). Samples were analyzed in Peakforce tapping mode with a Bruker Scanasyst fluid probe (nominal spring constant of 0.7 N/m).

For gel imaging, Fmoc-GFF solutions at different concentrations (1:12 and 1:16) were prepared by dissolving the gelator in the corresponding amounts of PBS buffer. A sample (40 μL) was cast onto a freshly cleaved mica disk, air-dried overnight, or dried under a gentle stream of nitrogen. Peakforce tapping mode with the Bruker Scanasyst air probe (nominal spring constant of 0.4 N/m) was used.

Small-angle neutron scattering (SANS) measurements were performed at Australia's Nuclear Science and Technology Organisation on the QUOKKA instrument. Hydrogel samples were prepared by dissolving Fmoc-GFF (1% (w/v)) in deuterated water. The samples were then vortexed, sonicated, and slightly warmed before transfer to a demountable titanium cell with a 2 mm path length to reach an ambient temperature. Data reduction was performed using IgorPro software and modeled using SasView.

3. RESULTS (WITH DISCUSSION)

3.1. Fmoc-GFF. To successfully form gel-core liposomes, identification of the appropriate gelation method is essential. However, this is complicated by partitioning of the gelator within the liposome. Several potential gelation methods were considered, such as salt screening using Dulbecco's modified Eagle's medium or a pH switch with slow glucono-δ-lactone hydrolysis. Ultimately, to avoid additional components and minimize system complexity, a temperature switch to induce gelation was employed. Higher temperatures disrupt the intermolecular interactions that form gels and increase the gelating molecule solubility; then, upon cooling, a one-dimensional self-assembly occurs.[23] To form gel-core liposomes, the peptides must be fully dispersed in the thin lipid film rehydration solution. To ensure Fmoc-GFF solubility in PBS, solution pH was investigated (pH 3−11.8). Gelation was triggered via the temperature switch approach, with gel formation monitored via the inversion test. Optimal pH values for temperature switch gel formation were found to be 7, 8, and 9. At these pH values, the Fmoc-GFF easily dissolved with sufficient gel formation in less than 2 h to withstand the inversion test. At low pH values (pH < 7), the gelator was insufficiently soluble, despite sonication, vortexing, and heating, thus rendering gels impossible under these conditions. Higher pH values (pH > 10), while solvating the gelator, greatly slowed the gelation rate (as observed using the inversion test) and presented the additional risk of cleaving the Fmoc capping group at high pH. The Fmoc-GFF dissolved well in PBS at a pH 10.0 and maintained the gelator in solution without gel formation, making it a good option for the liposome encapsulation process. Once encapsulated, gelation may then be initiated inside the liposomes, forming the gel-core liposomes, using dialysis to lower the pH to a physiologically relevant range.

Native gel sample topography imaging in liquids by AFM is a nontrivial task; thus, the Fmoc-GFF from PBS buffer at pH

https://doi.org/10.1021/acsanm.3c02172
ACS Appl. Nano Mater. 2023, 6, 14745−14755

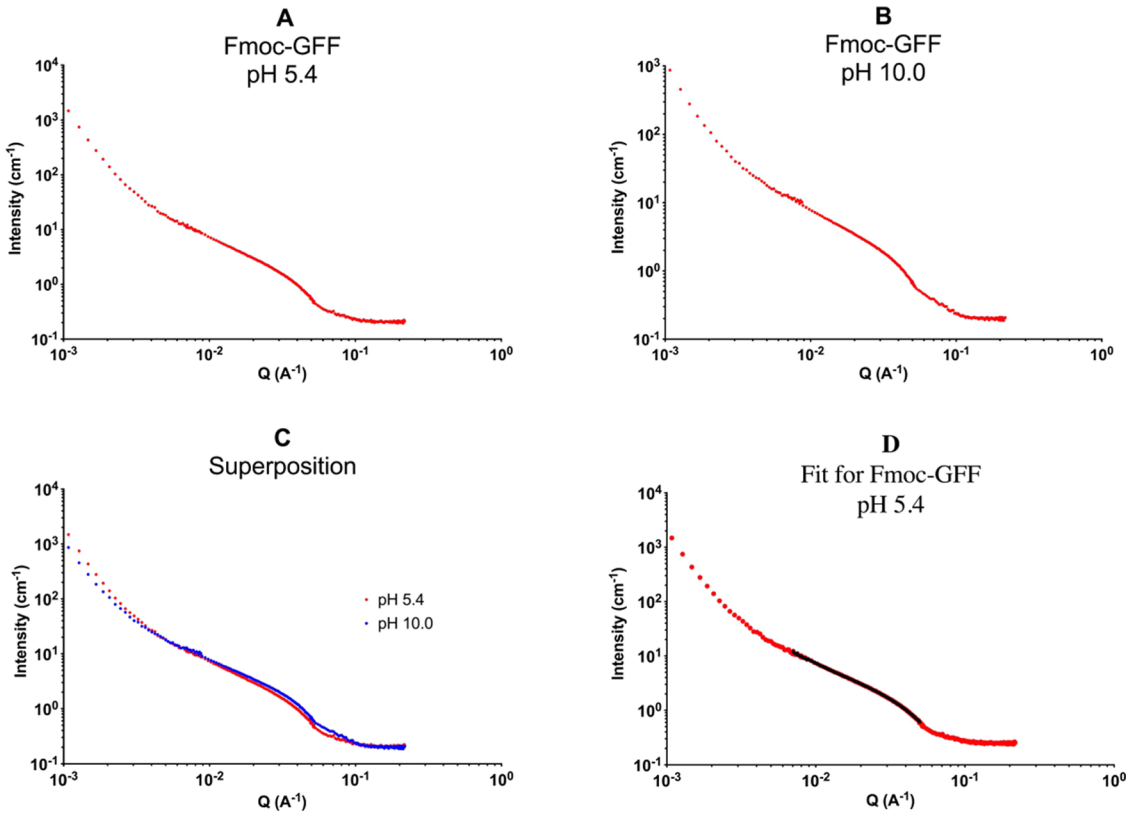

Figure 2. SANS scattering patterns for (A) Fmoc-GFF in 20 mM deuterated PBS buffer at pH 5.4 and (B) Fmoc-GFF in 20 mM deuterated PBS buffer at pH 10.0. Fmoc-GFF concentration: 1% (w/v). Panel (C) represents a superposition of both graphs. (D) Fmoc-GFF in 20 mM deuterated PBS buffer at pH 5.4 (red) and its fitted data using a flexible cylinder model (black).

7.4 fiber morphology was initially studied in the dry state using atomic force microscopy (Figure 1). The observed fibers appear flat, without coils and without branching. Fibers cross over each other and associate, forming bundles of up to three. Fiber diameters measured ranged between 11 and 25 nm. As features observed by AFM commonly appear wider than they are due to profile broadening artifacts, the diameter of cylindrical features is usually determined by height. However, for these films, imaging single fibers was impossible, even in the most dilute areas of the sample due to interference from residual buffer salts. The fiber diameter was therefore determined using other techniques to compliment the AFM measurements.

Small-angle neutron scattering (SANS) is one technique used to evaluate soft materials like gels and here was used to determine the Fmoc-GFF fiber radius. Fmoc-GFF was dissolved in a PBS buffer of deuterated water, vortexed, sonicated, and gently heated before being allowed to cool in a SANS cell and undergoing gelation. Samples were analyzed at 25 °C. Data obtained for Fmoc-GFF in deuterated PBS at pH 5.4 were compared to data for Fmoc-GFF in deuterated PBS at pH 10.0 (Figure 2). As the scattering data show, there is no significant difference between these two extremes with strong similarity between the data from both pH 5.4 and pH 10.0. The similarity of the SANS data indicates that at both pH values, similar structures exist and are likely to exist over the entire pH range between those two points, implying that these structures are also present at a pH of 7.4.

Data were modeled using a flexible cylinder model with parameters selected for each scattering pattern based upon the AFM data. The scattering length density (SLD) of the peptide was calculated to be 1.93×10^{-6} Å^{-2}, and that of the solvent (D_2O) was fixed at 6.3×10^{-6} Å^{-2}. Other parameters were allowed to vary freely, and following a few optimization cycles, the background was subtracted. Once this was complete, further parameter optimization was performed using multiple starting values for the Kuhn length, radius, and cylinder length and then minimized to ensure that a physically realistic global minimum was found.[24]

The scattering data were fitted to a flexible cylinder model using variables determined by AFM imaging, a method successfully employed in previous self-assembled peptide gel studies.[25,26]

The fitted data (chi-squared value of 0.990) gave a fiber radius of 35.2 Å—or 3.5 nm, a fiber length of 1483 Å (previous work points toward this being the average length between fiber overlap in the hydrogel and not the fiber physical length),[27] and a Kuhn length of 527.5 Å was obtained, indicating a flexible fiber. The fiber radius obtained is smaller than that obtained using AFM imaging (around 5−13 nm per bundle), but represents a more realistic radius as AFM profile broadening is avoided.

As previously mentioned, the similarity between scattering data for pH 5.4 and 10.0 suggests that within this range scattering patterns are independent of pH. This implies that the fundamental Fmoc-GFF gel structures exist at both pH values and thus are inferred to exist within the spectrum of pH values between. Overall, this supports the propensity for gel formation to occur within the liposome confines, indicating the potential of the Fmoc-GFF gelator to act as a structurally rigidifying component within gel-core liposomes.

https://doi.org/10.1021/acsanm.3c02172
ACS Appl. Nano Mater. 2023, 6, 14745−14755

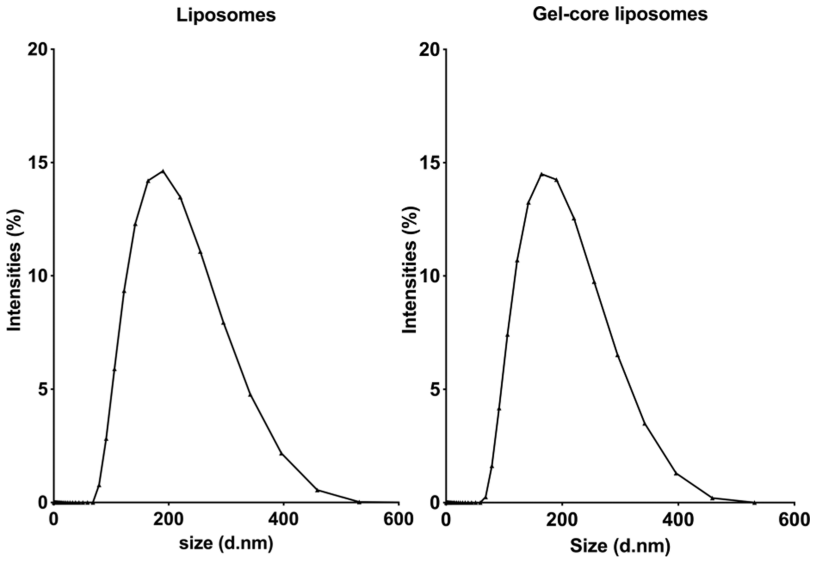

Figure 3. Left, DLS measurements on liposomes (0.15 mg/mL) in 20 mM phosphate buffer saline, pH 7.4, extruded through 400 and then 200 nm membranes. The *z*-average diameter of the aggregates is 173 ± 1 nm. Right, DLS measurements on liposomes (0.15 mg/mL) with Fmoc-GFF in their core in a 20 mM phosphate buffer saline, pH 7.4, extruded through 400 nm and then 200 nm membranes. The *z*-average diameter of the aggregates is 161 ± 1 nm.

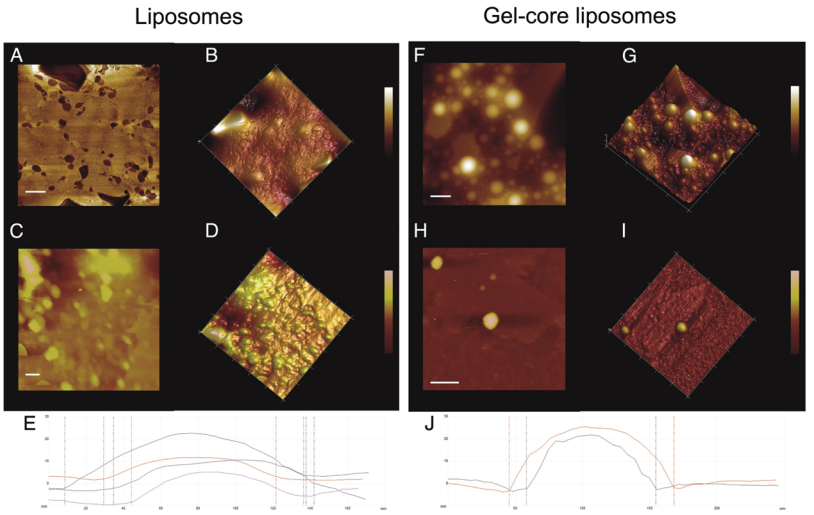

Figure 4. AFM on biotinylated liposomes (A–E) and gel-core biotinylated liposomes with 1% (w/v) Fmoc-GFF (F–J). (A, B) Imaging of a dry sample (MM8 AFM instrument) on a mica disk; 2D and 3D representations. Scale bar 100 nm. (C, D) Imaging of a liquid sample (catalyst AFM instrument) on a streptavidin-covered mica disk. 2D and 3D representations. Scale bar 100 nm. (E) Height section in liquid (catalyst) on a streptavidin-covered mica disk. Red: 90.2 nm, gray: 158.1 nm, purple: 105 nm, and pink: 91.4 nm. (F, G) Imaging a dry sample (MM8 AFM instrument) on a mica disk, 2D and 3D representations. Scale bar = 200 nm. (H, I) Imaging of a liquid sample (catalyst AFM instrument) on a streptavidin-covered mica disk; 2D and 3D representations. Scale bar is 200 nm. (J) Height section of the biotinylated liposomes in liquid (catalyst AFM instrument) on a streptavidin-covered mica disk. Red: 140.5 nm, gray: 113.8 nm.

3.2. Gel-Core Liposomes and Liposomes. To stabilize the liposome and gel-core liposome structures, a sterol, cholesterol, was added to the egg phosphatidylcholine to modulate the lipid bilayer fluidity. This increases the phospholipid-based liposome stability by preventing the crystallization of the acyl chain of the phospholipid, which provides steric hindrance to their movement. Ultimately, this reduces liposome permeability, making them more efficient drug delivery systems.[7] The subsequent liposomes (empty, containing the Fmoc-GFF gelator, or containing a perylene-based gelator) were analyzed using a variety of microscopy techniques. Transmission electron microscopy (TEM) and *cryo*-TEM were used to characterize the range of liposome sizes and shapes. Confocal microscopy was used to observe the successful encapsulation of a fluorescent gelator inside the liposomes. Atomic force microscopy (AFM) was used to compare the mechanical properties of liposomes and gel-core liposomes.

DLS was used to compare the liposome and gel-core liposome size and dispersity. When carried out on liposomes prepared at 0.15 mg/mL and then extruded (400 and then 200 nm), a relatively monodisperse sample was observed, as indicated by the presence of a single defined peak in the size distribution shown in Figure 3. The *z*-average diameter was found to be 173 ± 1 nm (maximum of 210 nm at max intensity) with a polydispersity index (PDI) of 0.1. The gel-

https://doi.org/10.1021/acsanm.3c02172
ACS Appl. Nano Mater. 2023, 6, 14745–14755

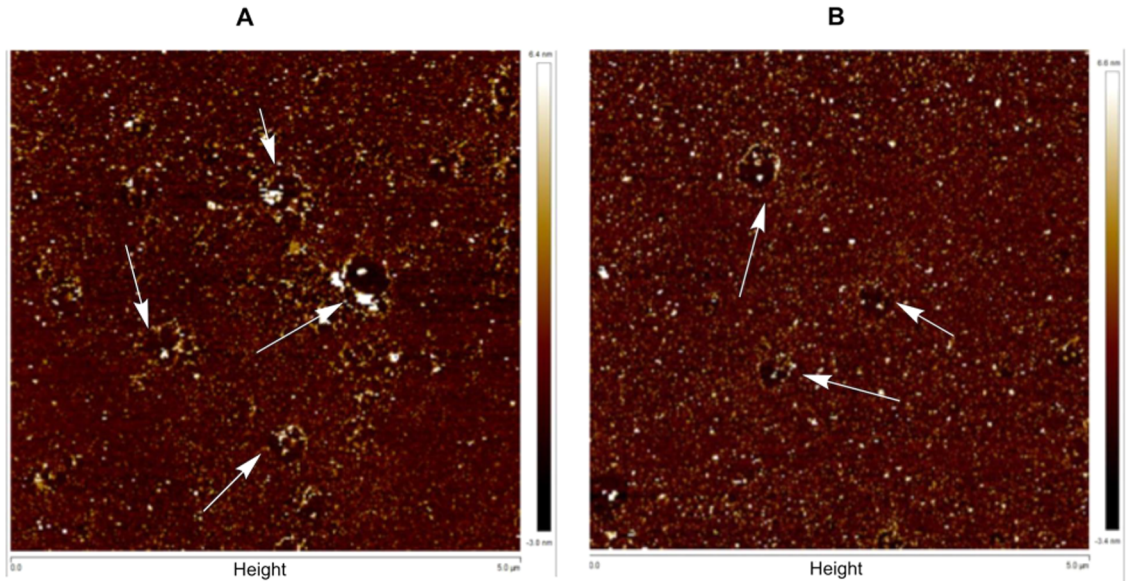

Figure 5. Images of AFM on (A) biotinylated liposomes in liquid (low *z*-range sample scanning) on a streptavidin-covered mica; (B) biotinylated gel-core liposomes in liquid (low *z*-range sample scanning) on a streptavidin-covered mica. The white arrows point out to the craters formed by liposomes before being washed away by the AFM tip.

core liposomes presented a monodisperse sample with a *z*-average diameter of 161 ± 1 nm (maximum of 190 nm at max intensity) and a PDI of 0.1, roughly 7% smaller than normal liposomes.

However, DLS does suffer from an extreme sensitivity to large particles.[28] The presence of a small number of large particles in a sample greatly skews the measurement, as they scatter significantly more light, dominating the signal. Thus, the mean-diameter is often overestimated. This sensitivity shows that DLS, although excellent for monodisperse samples, may give inaccurate results should particle size populations be nonideal. Hence, to obtain robust values for the liposome and gel-core liposome physical properties, multiple characterization techniques are necessary.

AFM was used to visualize both dried and native (wet) samples. Both techniques were employed to avoid artifacts that arise from the imaging of dry samples, as previously discussed, and to verify observations in the liquid state of materials that contain gels, which, as also previously discussed, are nontrivial materials to image. From comparisons of these analyses, a greater understanding will be obtained on the variations in sizes and shapes of liposomes and gel-core liposomes.[29] An additional advantage of AFM, for both dry and wet imaging, is that once liposomes and gel-core liposomes are located and imaged, physical evaluations such as surface nanoindentation can be performed.[30] Imaging liposomes in liquid, in the absence of surface or lipid modification, is a challenging task.[31] Thus, to facilitate liposome and gel-core liposome immobilization on the imaging substrate, biotinylated liposomal systems were used as well as nonmodified liposomal systems. Biotinylated liposomes were used only for AFM imaging. First, gel-free liposomes were imaged to evaluate liposome indentation. Data for the imaging of gel-free biotinylated liposomes is shown in Figures 4A−E and 5A. Imaging of dry gel-free liposome samples shows only large or very angular aggregates of dried lipids (Figure 4A,B), presenting very little resemblance to the expected liposome structure (confirmed by DLS and TEM, shown later). This disparity between the observed and expected liposomal structure is hypothesized to be due to sample preparation effects. Particularly, the drying step, which may cause liposomes to adhere, forms large aggregates. Dry AFM of liposomes gave a population with an average size of 35 nm (median of 34 nm, standard error of mean of 2 nm). Liquid imaging with a small *z*-range (2.5 mm) revealed craters (Figure 5A), which may indicate previous liposome adhesion sites, resulting from a destructive interaction between the AFM tip and liposome during scanning. With a larger *z*-range (20 mm), spherical structures between 50 and 150 nm in diameter and 10−40 nm in height are observed (Figure 4C,D). The discrepancy between the height and diameter may be due to profile broadening artifacts, a combination of sample concentration variation over time, and physical deformation of the soft liposomal structures upon interaction with the AFM tip. In this situation, liposome physical deformation may be exacerbated as the membrane-bound biotin irreversibly binds to the functionalized AFM substrate. With each deformation, induced upon interaction between the AFM tip and flexible liposome, the liposome is progressively flattened as it associates with the surface. This technique gave a liposome population with an average size of 64 nm (median 60 nm standard error of 4 nm).

These data indicate that even with surface immobilization via biotinylation, AFM imaging on gel-free liposomes is challenging and does not yield reliably accurate characterization data. Contrary to gel-free liposomes, dry samples of the gel-core liposomes were much simpler to image by AFM (Figure 4F,G), with spherical structures clearly visible. The structural rigidity enabling observation by AFM is likely due to the core of the gel-core liposomes. The solid-like core material appears to confer a resistance to deformation during the drying process and to indentation by the AFM tip. Dry AFM of liposomes containing Fmoc-GFF gave a population with an average size of 115 nm (median of 108 nm, standard error of the mean of 5 nm). Similarly, when imaged in liquid with a low *z*-range sample scanning instrument (Figure 5B), these gel-core liposomes displayed the same features as observed for the gel-free liposomes. The presence of craters indicates that gel-core liposomes were located in that area; however, the AFM

https://doi.org/10.1021/acsanm.3c02172
ACS Appl. Nano Mater. 2023, 6, 14745−14755

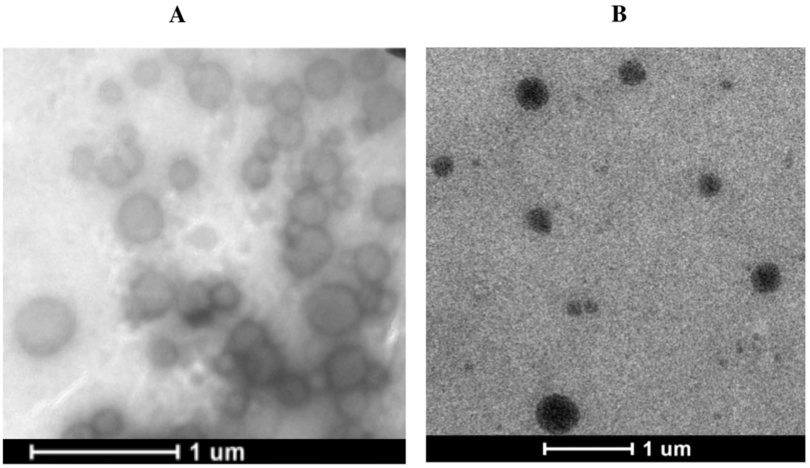

Figure 6. (A) Stained transmission electron micrographs of gel-core liposomes (15 mg/mL) containing a solution of a perylene gelator in PBS buffer (20 mM, pH 10.0). (B) Unstained transmission electron micrographs of gel-core liposomes (15 mg/mL) containing a solution of perylene gelator in PBS buffer (20 mM, pH 10.0). Images were taken on a Tecnai microscope (200 kV).

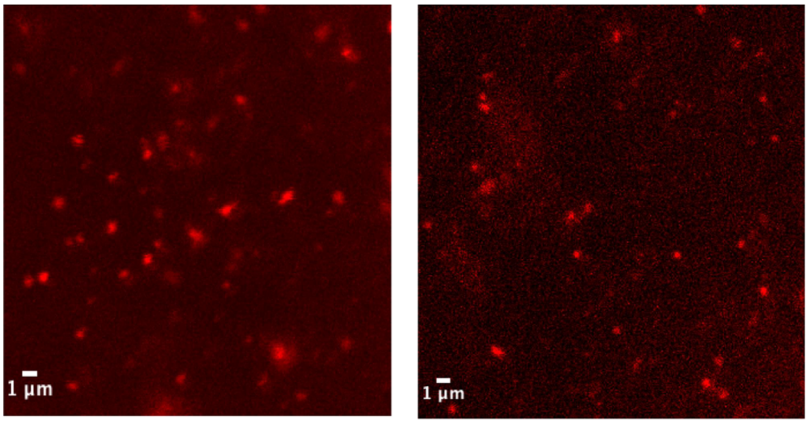

Figure 7. Confocal microscopy images of gel-core liposomes (15 mg/mL) prepared in a solution of a perylene gelator in PBS buffer (20 mM, pH 10.0) after dialysis against PBS (20 mM, pH 5.4). The resulting gel-core liposomes were diluted to 1% of their initial concentration and then immobilized prior to imaging in a nonfluorescent 1% (w/v) Fmoc-GFF gel. Images taken on a Leica SP5 2P STED using a 100.0 × 1.40 oil objective at room temperature.

tip again appears to be destructively interacting with the gel-core liposomes. This is likely similar to the behavior observed for the gel-free liposomes. When a higher *z*-range sample scanning was used (Figure 4H,I), gel-core liposomes were successfully observed on the substrate as spherical structures with a diameter of roughly 130 nm (median 127 nm, standard error of mean 19 nm). For the liposomes and gel-core liposomes that remained spherical, there was no significant difference in their heights, as measured by AFM. However, the gel-free liposomes tended to flatten more easily than when filled with a gel. This is especially noticeable with dry sample AFM imaging. The biotin distributed over the membrane interacting with the streptavidin-treated surface as the AFM tip moved influenced the shape of the liposomes, possibly flattening the liposomes over time. From these observations, the incorporation of a gel-core to the liposomes confers significantly greater physical stability and prevents deformation of these structures caused by the AFM tip.

Further supporting evidence for gelator encapsulation inside the liposomes was obtained by using TEM, *cryo*-TEM, and confocal microscopy. Negatively staining liposomes for TEM imaging using a uranyl acetate solution is necessary as phospholipids have poor electron-scattering properties and are not visible in the micrographs. The negatively stained TEM micrographs of gel-core liposomes containing Fmoc-GFF only showed a black spherical structure (Supporting Information Figure 1; average size 326 nm, median 318 nm, standard error of mean 19 nm). Unstained samples were also imaged (Supporting Information Figure 2), the micrographs of which revealed no discernible features. No proof of gel encapsulation could therefore be made using the Fmoc-GFF as the only observable feature was the staining of liposome membranes.

Contrary to Fmoc-GFF, the perylene gelator is both optically active and a good electron acceptor in solution. This electron acceptor capability results in a greater capacity for the gel component to absorb electrons from an electron beam, creating a contrast in the TEM imaging. This means that gel-core liposomes made using the perylene gelator should image well in TEM. Prior to imaging, the liposomal solution containing the perylene gelator was dialyzed to ensure full removal of any nonencapsulated gelator. Negatively stained samples were compared to the unstained samples. For both stained and unstained samples (Figure 6), spherical structures of roughly 200 nm (stained: 261 nm, median 260 nm, standard error of mean 12 nm, unstained: 204 nm, median 175 nm,

https://doi.org/10.1021/acsanm.3c02172
ACS Appl. Nano Mater. 2023, 6, 14745−14755

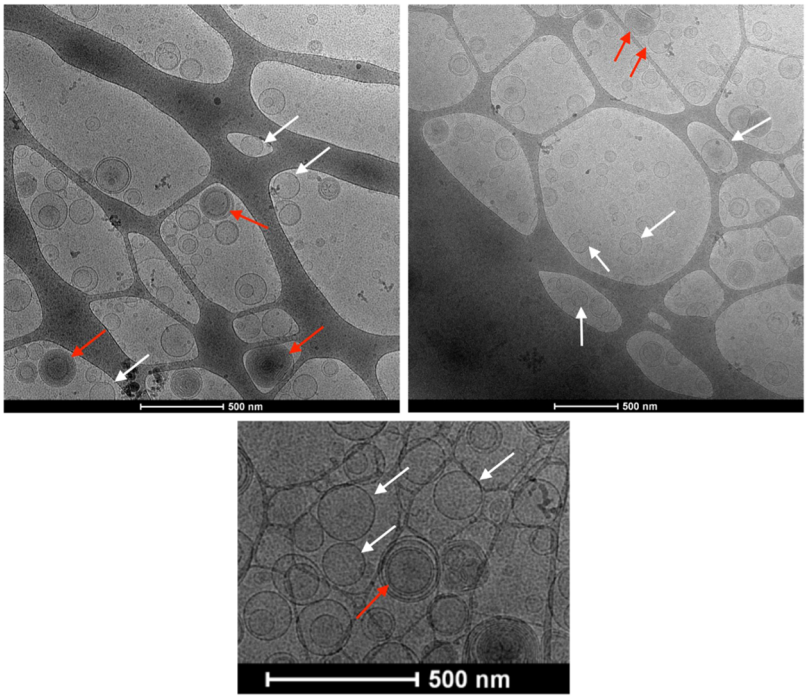

Figure 8. *Cryo*-TEM images of gel-core liposomes (15 mg/mL) containing the Fmoc-GFF gelator. The white arrows point to unilamellar liposomes, while red arrows point to multilamellar liposomes. Images taken on a Tecnai microscope (200 kV).

standard error of mean 15 nm) scattered across the stained grids are observed. This demonstrates that the presence of a perylene gelator does not hinder liposome formation. In the stained micrographs (Figure 6A), the phospholipid shells are clearly distinguishable as the uranyl acetate solution preferentially stains the membrane. When the samples are imaged in the absence of negative staining, the membranes are no longer visible on the micrographs (Figure 6B) but spherical structures, liposomes, are still apparent thanks to the encapsulation of the perylene gelator. There is relatively good agreement between the sizes obtained using DLS and TEM (same order of magnitude). However, some variations in TEM may be due to sample preparation.

Interestingly, imaging of stained (diameter including the membrane) and unstained (diameter not including the membrane) gel-core liposomes using TEM can give an approximate volume of the inside of a liposome as well as an approximate volume of the shell. Using the $V = \frac{4}{3}\pi r^3$ formula, a shell volume of roughly 5 mm^3 was obtained, with a volume of core encapsulation of roughly 4 mm^3. This information can prove to be important for further encapsulation studies.

Further evidence supporting gel encapsulation was obtained by using confocal fluorescence microscopy (Figure 7). Gel-core liposome samples made incorporating the fluorescent perylene gelator (of a bright red color) were diluted to 1% of their initial concentration into a gel formed from 1% (w/v) nonfluorescent Fmoc-GFF to create an immobile matrix that was imaged by confocal microscopy. Images of these samples showed bright red spherical structures, which are assumed to be the encapsulated perylene gelator, forming the gel-core liposomes. As the perylene dye fluorescence is very strong, a 1% solution made of the original liposomal solution is necessary as to not saturate with the perylene fluorescence.

As with the TEM micrographs, the particle size observed using confocal microscopy (100−600 nm, with an average of 342 nm, a median of 346 nm, and a standard error of mean of 20 nm) differed from the average size obtained using DLS (160−180 nm depending on the batch). This is likely due to the ultimate resolution limit of the microscope according to Abbe's law (200−300 nm).

A common challenge encountered in imaging liposomes and gel-core liposomes, resulting in size discrepancies, is partially attributable to the drying effect. An imaging technique that may avoid this issue is cryogenic transmission electron microscopy. This technique enables liposome imaging in a snap-frozen aqueous solution, which should side-step the drying issues and provide results that may validate liquid AFM imaging. This technique eliminates the need for negative staining and drying of the samples and allows analysis in a native solution state. Gel-core liposome samples for *cryo*-TEM were plunged into liquid ethane at −183 °C and cooled using liquid nitrogen. During this snap-freezing step, the nanostructures are instantaneously embedded in vitrified amorphous ice, trapping them in a near-native hydrated state.[32] Figure 8 presents typical *cryo*-TEM images of the gel-core liposomes encapsulating Fmoc-GFF (which has poor electron-scattering properties) in their core. Some observed gel-core liposomes appear to be multilamellar (red arrows in Figure 8), instead of unilamellar (white arrows). This may be due to negatively charged impurities, present in naturally isolated egg-PC, which disrupted and complicated liposome formation.[33] However, more than 75% of the liposomes obtained were unilamellar.

The gel-core liposomes observed in the *cryo*-TEM images appear to be somewhat smaller than 200 nm in diameter, averaging a size of around 131 nm, with a median of 127 nm and a standard error of the mean of 10 nm agreeing with the DLS results in Figure 3. This supports the hypothesis that drying of the liposomes and negative staining is responsible for the size variations between imaging techniques.

https://doi.org/10.1021/acsanm.3c02172
ACS Appl. Nano Mater. 2023, 6, 14745−14755

Table 1. Summary of the Population Studies Done on the Data Obtained While Characterizing Liposomes and Gel-Core Liposomes Using Several Techniques[a]

system	N	min (nm)	max (nm)	mean (nm)	median (nm)	std dev (nm)	std error of mean (nm)	CI of mean (nm)
TEM (liposomes)	30	125	325	196	188	51	9	177−215
TEM (Fmoc-GFF stained)	10	228	429	326	318	60	19	283−369
TEM (perylene Unstained)	38	79	517	204	176	89	14	174−233
TEM (perylene stained)	39	128	423	261	260	76	12	237−286
AFM (liposome liquid)	18	42	92	64	69	17	4	56−73
AFM (liposome dry)	33	19	66	35	34	12	2	31−39
AFM (Fmoc-GFF liquid)	2	114	141	127	127	19	13	−43−297
AFM (Fmoc-GFF dry)	33	63	197	115	108	30	5	104−126
cryo-TEM (Fmoc-GFF)	24	54	243	131	127	49	10	110−151
confocal (perylene)	36	71	679	342	346	123	20	301−384
DLS (liposomes)	n/a	n/a	n/a	173	n/a	n/a	n/a	n/a
DLS	n/a	n/a	n/a	161	n/a	n/a	n/a	n/a

[a]*N* indicates the population counted; min is the size of the smallest structure; max is the size of the biggest structure; std dev is the standard deviation of the sample; std error of mean is the standard error of the mean of the samples; and CI of mean represents the 95% confidence interval of the mean of the sample.

Using hydrogen/deuterium contrast matching methods, SANS measurements were attempted to investigate the aggregate formed by the gelator in the core of the Fmoc-GFF gel-core liposomes to see whether the gelator formed a gel or stays solvated. These measurements were not sensitive enough to obtain a clear signal, and the incorporation of deuterated lipids changed the liposome system drastically. More information on this can be found in the Supporting Information.

3.2.1. Comparison and Contrasting of the Different Techniques Used to Characterize Liposomes and Gel-Core Liposomes. As shown throughout this study, several different techniques were used to try and analyze gel-core liposomes and compare them to normal (empty) liposomes. Table 1 shows the different population studies obtained from these various techniques (distribution plots can be found in the Supporting Information).

Liposomes (empty) were found to have statistically different mean sizes (see the Supporting Information) between the different technique used (196, 64, and 35 nm). It is important to note that the value obtained from TEM (196 nm, dry sample) is the closest to the value obtained via DLS (173 nm, native sample).

Gel-core liposome samples measured using *cryo*-TEM (131 nm, native sample) and using AFM in liquid (127 nm, native but modified using biotin) gave mean sizes very close to that obtained via DLS (161 nm, native sample), indicating that these methods might be the most appropriate to obtain a clearer picture of gel-core liposomes.

It is of importance to also note here that the population of gel-core liposomes, contrary to that of liposomes (empty), analyzed using dry and liquid AFMs did not present a statistical difference, indicating that adding a gel-core to liposomes may result in greater size homogeneity than when empty.

Similar to hydrogels, nanoscale composite systems (such as the gel-core liposomes presented in this work) are difficult to characterize using a single technique and require a combination of techniques to obtain a clear understanding of their sometimes contrasting and complex properties.

4. CONCLUSIONS

In summary, this study demonstrated the simple formation and promising properties achievable by gel-core liposomes using the small self-assembled peptide hydrogel Fmoc-GFF. The liposomes and gel-core liposomes were extensively characterized and evaluated. Due to the complicated structure of these nanoscale gel-core liposomes, a range of techniques were required to adequately characterize them. To evaluate the two different component features, namely, the liposome and the gel-core liposomes, no single technique is capable of fully evaluating each important property; indeed, the use of some imaging techniques necessitates destructive sample preparation (for example, sample drying for imaging). To overcome the challenges posed by the nanostructural complexity of these materials, an array of advanced imaging techniques are necessary and often yield varied results. Techniques such as TEM, *cryo*-TEM, AFM, and DLS provide different average sizes for liposomes and gel-core liposomes. Only *cryo*-TEM, and to some extent AFM of liquid samples, provides reliable (free of skewed particle size sensitivities) data for the native (nondried and unmodified in the case of *cryo*-TEM) structures. The variation in results obtained by various techniques confirms the influence of sample drying in inducing size discrepancies and highlights the importance of native imaging. AFM images in liquid gave data more consistent with the expected physical properties of the liposome and gel-core liposome structures and other liquid-based characterization techniques compared to techniques involving sample drying. However, imaging of dried biotinylated Fmoc-GFF gel-core liposome samples was more readily obtained than those of the gel-free liposomes, indicating significant structural rigidity conferred by the gel-core in preventing the destructive deformation of these structures caused by interactions with the AFM tip. Solution AFM images of the Fmoc-GFF gel-core biotinylated liposomes showed spherical structures of roughly 130 nm. Comparison of the liposome and gel-core liposome highlighted the greater tendency of liposomes to flatten out compared to the gel-core liposomes. Thus, liposome structural integrity is greatly improved by the inclusion of a gel-core.

More importantly, with the ease at which the highly complex gel-core liposome structure can be created, it can now be applied to a wide variety of new applications, from increasing the stability and shelf life of cosmetics and medicines, as well as

https://doi.org/10.1021/acsanm.3c02172
ACS Appl. Nano Mater. 2023, 6, 14745−14755

compartmentalizing storing molecules for potential nanosized chemical reactors. The next step in exploring these easily synthesized, yet highly complex materials, involves evaluating the compartmentalizing capacity, solution stability, and influence on the lifetime of sensitive compounds stored within the gel-core compartment of the liposome.

These nanoscale systems also have clinical applications and are viable, stable delivery systems. When dispersed in a gel matrix (creating gel-core liposomes within a gel), a slow controlled release profile of fluorescein was obtained,[22] in opposition to the burst release traditionally observed with gel delivery. Delivery through skin is also promising and will be the subject of further studies.[22]

■ ASSOCIATED CONTENT

Supporting Information

The Supporting Information is available free of charge at https://pubs.acs.org/doi/10.1021/acsanm.3c02172.

> Further transmission electron micrographs of liposomes and gel-core liposomes (Figures S1−S3), further explanation and scattering patterns (Figure S4) of small-angle neutron scattering experiments done on liposomal systems; stability studies performed on liposomes and gel-core liposomes (Table S1); and rheological data for Fmoc-GFF at 0.5 wt %, as well as a summary table (Table S2) of the plot distributions and results of Mann−Whitney tests of samples of liposomes and gel-core liposomes obtained using different characterization techniques (PDF)

■ AUTHOR INFORMATION

Corresponding Author

Geneviève Duché − *School of Chemistry, The University of New South Wales, Sydney 2052 NSW, Australia; Australian Centre for Nanomedicine, The University of New South Wales, Sydney 2052 NSW, Australia;* Present Address: Génie Enzimatique et Cellulaire, Université Technologique de Compiègne, Compiègne 60200, France; orcid.org/0000-0002-2966-7699; Email: gen.duche@yahoo.fr

Authors

Celine Heu − *Katharina Gaus Light Microscopy Facility, UNSW Mark Wainwright Analytical Centre, Sydney 2052 NSW, Australia*

Pall Thordarson − *School of Chemistry, The University of New South Wales, Sydney 2052 NSW, Australia; Australian Centre for Nanomedicine, The University of New South Wales, Sydney 2052 NSW, Australia; UNSW RNA Institute, The University of New South Wales, Sydney 2052 NSW, Australia;* orcid.org/0000-0002-1200-8814

Complete contact information is available at: https://pubs.acs.org/10.1021/acsanm.3c02172

Author Contributions

The manuscript was written through contributions of all authors. All authors have given approval to the final version of the manuscript.

Notes

The authors declare no competing financial interest.

■ ACKNOWLEDGMENTS

The authors would like to thank the Mark Wainwright Analytical Centre (UNSW) for access to instruments and the Australian Nuclear Science and Technology Organization (ANSTO) for access to the QUOKKA beamline (proposal 6041). The authors would also like to thank Dr. Adam Martin for his help at ANSTO and with SANS data. The authors received funding from the Australian Postgraduate Awards (APA) to GD and the Australian Research Council (ARC) (CE140100036 and DP190101892) to PT.

■ ABBREVIATIONS

AFM, atomic force microscopy; DLS, dynamic light scattering; Fmoc-GFF, Fmoc glycine diphenylalanine; HPLC, high-performance liquid-chromatography; PBS, phosphate buffer solution; PC, phosphatidylcholine; SANS, small-angle neutron scattering; TEM, transmission electron microscopy

■ ADDITIONAL NOTE

[1]This gelator was kindly provided by Dr Jonathan Wojciechowski, then a member of the School of Chemistry, UNSW.

■ REFERENCES

(1) Cevc, G. Lipid Vesicles and Other Colloids as Drug Carriers on the Skin. *Adv. Drug Delivery Rev.* **2004**, *56*, 675−711.

(2) Truong, W. T.; Su, Y.; Meijer, J. T.; Thordarson, P.; Braet, F. Self-Assembled Gels for Biomedical Applications. *Chem. - Asian J.* **2011**, *6*, 30−42, DOI: 10.1002/asia.201000592.

(3) Hsu, S. M.; Lin, Y. C.; Chang, J. W.; Liu, Y. H.; Lin, H. C. Intramolecular Interactions of a Phenyl/Perfluorophenyl Pair in the Formation of Supramolecular Nanofibers and Hydrogels. *Angew. Chem., Int. Ed.* **2014**, *53*, 1921−1927.

(4) Calixto, G.; Yoshii, A. C. Rocha E Silva, H.; Stringhetti Ferreira Cury, B.; Chorilli, M. Polyacrylic Acid Polymers Hydrogels Intended to Topical Drug Delivery: Preparation and Characterization. *Pharm. Dev. Technol.* **2015**, *20*, 490−496.

(5) Sengupta, S.; Banerjee, S.; Sinha, B.; Mukherjee, B. Improved Skin Penetration Using In Situ Nanoparticulate Diclofenac Diethylamine in Hydrogel Systems: In Vitro and In Vivo Studies. *AAPS PharmSciTech* **2016**, *17*, 307−317.

(6) El-Refaie, W. M.; Elnaggar, Y. S. R.; El-Massik, M. A.; Abdallah, O. Y. Novel Self-Assembled, Gel-Core Hyaluosomes for Non-Invasive Management of Osteoarthritis: In-Vitro Optimization, Ex-Vivo and In-Vivo Permeation. *Pharm. Res.* **2015**, *32*, 2901−2911.

(7) Mozafari, M. R. Nanoliposomes:preparation and analysis. In *Liposomes. Methods in Molecular Biology (Methods and Protocols)*; Weissig, V., Ed.; Humana Press, 2010; pp 29−50.

(8) Akbarzadeh, A.; Rezaei-Sadabady, R.; Davaran, S.; Joo, S. W.; Zarghami, N.; Hanifehpour, Y.; Samiei, M.; Kouhi, M.; Nejati-Koshki, K. Liposome: Classification, Preparation, and Applications. *Nanoscale Res. Lett.* **2013**, *8*, 102.

(9) Petralito, S.; Spera, R.; Pacelli, S.; Relucenti, M.; Familiari, G.; Vitalone, A.; Paolicelli, P.; Casadei, M. A. Design and Development of PEG-DMA Gel-in-Liposomes as a New Tool for Drug Delivery. *React. Funct. Polym.* **2014**, *77*, 30−38.

(10) El-Refaie, W. M.; Elnaggar, Y. S. R.; El-Massik, M. A.; Abdallah, O. Y. Novel Curcumin-Loaded Gel-Core Hyaluosomes with Promising Burn-Wound Healing Potential: Development, in-Vitro Appraisal and in-Vivo Studies. *Int. J. Pharm.* **2015**, *486*, 88−98.

(11) Liu, Y.; Liang, D. Hydrogel Integrated with Liposome: A Two-Stage Drug Delivery System. *J. Controlled Release* **2011**, *152*, e63−e64.

(12) Tiwari, S.; Goyal, A.; Khatri, K.; Mishra, N.; Vyas, S. Gel Core Liposomes: An Advanced Carrier for Improved Vaccine Delivery. *J. Microencapsulation* **2009**, *26*, 75−82, DOI: 10.1080/02652040802170897.

(13) Liu, D.; Angelova, A.; Liu, J.; Garamus, V.; Angelov, B.; Zhang, X.; Li, Y.; Feger, G.; Li, N.; Zou, A. Self-Assembly of mitochondria-specific Peptide Amphiphiles Amplifying Lung Cancer Cell Death Through Targeting the VDAC1-hexokinase-II Complex. *J. Matter. Chem. B* **2019**, *7*, 4706−4716.
(14) Angelova, A.; Dreschsler, M.; Garamus, V.; Angelov, B. Pep-Lipid Cubosomes and Vesicles Compartmentalized by Micelles from Self-Assembly of Multiple Neuroprotective Building Blocks Including a Large Peptide Hormone PACAP-DHA. *ChemNanoMat* **2019**, *5*, 1381−1389.
(15) Ischakov, R.; Adler-Abramovich, L.; Buzhansky, L.; Shekhter, T.; Gazit, E. Peptide-Based Hydrogel Nanoparticles as Effective Drug Delivery Agents. *Bioorg. Med. Chem.* **2013**, *21*, 3517−3522.
(16) Martin, A. D.; Robinson, A. B.; Mason, A. F.; Wojciechowski, J. P.; Thordarson, P. Exceptionally Strong Hydrogels through Self-Assembly of an Indole-Capped Dipeptide. *Chem. Commun.* **2014**, *50*, 15541−15544.
(17) Mahler, A.; Reches, M.; Rechter, M.; Cohen, S.; Gazit, E. Rigid, Self-Assembled Hydrogel Composed of a Modified Aromatic Dipeptide. *Adv. Mater.* **2006**, *18*, 1365−1370.
(18) Reches, M.; Gazit, E. Self-assembly of peptide nanotubes and amyloid-like structures by charged-termini capped diphenylalanine peptide analogues. *Isr. J. Chem.* **2005**, *45*, 363−371.
(19) Jayawarna, M.; Ali, M.; Jowitt, T. A.; Miller, A. F.; Saiani, A.; Gough, J. E.; Ulijn, R. V. Nano-structure Hydrogels for 3D Cell Culture through Self-Assembly of Fmoc-dipeptides. *Adv. Mater.* **2006**, *18*, 611−614.
(20) Wojciechowski, J. P.; Martin, A. D.; Mason, A. F.; Fife, C. M.; Sagnella, S. M.; Kavallaris, M.; Thordarson, P. Choice of Capping Group in Tripeptide Hydrogels Influences Viability in the Three-Dimensional Cell Culture of Tumor Spheroids. *ChemPlusChem* **2017**, *82*, 383−389.
(21) Johnson, E. K.; Adams, D. J.; Cameron, P. J. Peptide Based Low Molecular Weight Gelators. *J. Mater. Chem.* **2011**, *21*, 2024−2027.
(22) Duché, G. Encapsulating self-assembled peptide hydrogels in liposomes for drug delivery and aesthetic therapy Ph.D. Dissertation; University of New South Wales: Australia, 2019.
(23) Korevaar, P. A.; Newcomb, C. J.; Meijer, E. W.; Stupp, S. I. Pathway Selection in Peptide Amphiphile Assembly. *J. Am. Chem. Soc.* **2014**, *136*, 8540−8543.
(24) McEwen, H.; Du, E. Y.; Mata, J. P.; Thordarson, P.; Martin, A. D. Turning Hydrogels through Metal-Base Gelation Triggers. *J. Mater. Chem. B* **2017**, *5*, 9412−9417.
(25) Martin, A. D.; Wojciechowski, J. P.; Robinson, A. B.; Heu, C.; Garvey, C. J.; Ratcliffe, J.; Waddington, L. J.; Gardiner, J.; Thordarson, P. Controlling Self-Assembly of Diphenylalanine Peptides at High PH Using Heterocyclic Capping Groups. *Sci. Rep.* **2017**, *7*, No. 43947.
(26) SasView User Documentation, Model Functions. Flexible cylinder (accessed Oct 3, 2018) http://www.sasview.org/docs/user/models/flexible_cylinder.html.
(27) Barker, E. C.; Martin, A. D.; Garvey, C. J.; Goh, C. Y.; Jones, F.; Mocerino, M.; Skelton, B. W.; Ogden, M. I.; Becker, T. Thermal Annealing Behaviour and Gel to Crystal Transition of a Low Molecular Weight Hydrogelator. *Soft Matter* **2017**, *13*, 1006−1011.
(28) Anderson, W.; Kozak, D.; Coleman, V. A.; Jämting, ÅK.; Trau, M. A Comparative Study of Submicron Particle Sizing Platforms: Accuracy, Preci- _Sion and Resolution Analysis of Polydisperse Particle Size Distribution. *J. Colloid Interface Sci.* **2013**, *405*, 322−330.
(29) Alfonta, L.; Singh, A. K.; Willner, I. Liposomes Labeled with Biotin and Horseradish Peroxidase: A Probe for the Enhanced Amplification of Antigen − Antibody or Oligonucleotide − DNA Sensing Processes by the Precipitation of an Insoluble Product on Electrodes. *Anal. Chem.* **2001**, *73*, 91−102.
(30) Et-Thakafy, O.; Delorme, N.; Gaillard, C.; Mériadec, C.; Artzner, F.; Lopez, C.; Guyomarch, F. Mechanical Properties of Membranes Composed of Gel-Phase or Fluid-Phase Phospholipids Probed on Liposomes by Atomic Force Spectroscopy. *Langmuir* **2017**, *33*, 5117−5126.
(31) Teschke, O.; De Souza, E. F. Liposome Structure Imaging by Atomic Force Microscopy: Verification of Improved Liposome Stability during Adsorption of Multiple Aggregated Vesicles. *Langmuir* **2002**, *18*, 6513−6520.
(32) McDowall, A. W.; Chang, J. J.; Freeman, R.; Lepault, J.; Walter, C. A.; Dubochet, J. Electron Microscopy of Frozen Hydrated Sections of Vitreous Ice and Vitrified Biological Samples. *J. Microsc.* **1983**, *131*, 1−9.
(33) Dimitrova, M. N.; Tsekov, R.; Matsumura, H.; Furusawa, K. Size Dependence of Protein-Induced Flocculation of Phosphatidylcholine Liposomes. *J. Colloid Interface Sci.* **2000**, *226*, 44−50.

https://doi.org/10.1021/acsanm.3c02172
ACS Appl. Nano Mater. 2023, 6, 14745−14755